Geophys. J. Int. (2007) **170,** 1227–1242 doi: 10.1111/j.1365-246X.2007.03473.x

Seismic wave properties in time-dependent porosity homogeneous media

G. Quiroga-Goode, R. Padilla-Hernández and S. Jiménez-Hernández

Instituto de Investigación en Ingeniería, Universidad Autónoma de Tamaulipas, Tampico, México 89330*, México. E-mail: gquirogagoode@netscape.net*

Accepted 2007 April 23. Received 2007 April 20; in original form 2005 June 6

SUMMARY

It is quantified the properties of seismic waves in fully saturated homogeneous porous media within the framework of Sahay's modified and reformulated poroelastic theory. The computational results comprise amplitude attenuation, velocity dispersion and seismic waveforms. They show that the behaviour of all four waves modelled as a function of offset, frequency, porosity, fluid viscosity and source bandwidth depicts realistic dissipation within the sonic–ultrasonic band. Therefore, it appears that there is no need to include material heterogeneity to model attenuation. By inference it is concluded that the fluid viscosity effects may be enhanced by dynamic porosity.

Key words: dynamic porosity, slow *P* wave, slow *S* wave.

1 INTRODUCTION

The dynamics of porous media has been extensively studied from several standpoints, including granular medium theories (Bhattacharyya 1965; Godano & Oliveri 1999), mixture theories (Corapcioglu & Tuncay 1996), poroelastic theories (below), among others. The latter has been analysed from mainly two perspectives. The first is represented by the large body of work associated to Biot (Biot 1956, 1962; White 1975; Bourbie *et al.* 1987; Pride *et al.* 1992; Dvorkin *et al.* 1994; Carcione & Quiroga-Goode 1995). The second corresponds to de la Cruz and Spanos theory (de la Cruz & Spanos 1985, 1989; de la Cruz *et al.* 1993; Hickey 1994; Hickey *et al.* 1995; Sahay 1996; Sahay *et al.* 2001; Sahay 2001; Quiroga-Goode *et al.* 2005).

The key difference between the two is that they are derived from different approaches. On the one hand, de la Cruz and Spanos theory obtains macroscopic continuity and constitutive relations and field equations by volume averaging the underlying pore-scale motions. Biot on the other hand, first postulated expressions for the kinetic, strain and dissipative energy functions, and later obtained the kinetic and strain energy equations by approximate volume averaging of the energies in each phase. Both methods arrive at macroscopic descriptions of the dynamics of porous media that are comparable on the whole, provided some assumptions are met. The physical validity of the model was confirmed by macroscopic thermodynamics (de la Cruz *et al.* 1993).

While Biot did not consider porosity as an independent field, his theory implicitly predicts the time-dependent behaviour of porosity. Assuming large porosity relaxation times compared to wave propagation, the changes of porosity are present in Biot theory via $\partial_t \eta = (\eta_0 \delta + \Phi)\nabla \cdot v^s - \Phi \nabla \cdot v^f$ (Wilmanski 2006), where ∂_t represents the time differential operator, η dynamic porosity and η_0 its constant counterpart. The material parameters δ and Φ can be related to compressibilities of materials by means of the same Gedanken experiments which yield to Gassmann relations. Finally, $\mathbf{v}^s$ and $\mathbf{v}^f$ correspond to the particle velocities of the solid and fluid, respectively.

As far as form is concerned, Biot porosity equation is essentially the same as that of de la Cruz and Spanos $\partial_t \eta = \delta_s \nabla \cdot v^s - \delta_f \nabla \cdot v^f$ provided that $\delta_s = \eta_0 \delta + \Phi$ and $\delta_f = \Phi$. Here, δ_s and δ_f correspond, respectively, to the solid and fluid compliances (Appendix A). Therefore, the key issue is not that dynamic porosity is entirely absent in Biot theory, but that it is missing in his derivation of elastic energy potential, from which the solid and fluid stresses can be obtained by differentiation with respect to the strains. For Biot's use of potential energy to be valid, it would be necessary that $\delta_s = \delta_f = 0$ (or, by the same token, $\delta = \Phi = 0$), but they can be determined from measurable compressibilities and are demonstrably non-zero (Hickey *et al.* 1995). The ultimate outcome is that velocity dispersion and amplitude attenuation appear to be underestimated (Sahay 2001).

To make up for the missing attenuation in Biot theory, several modifications and adaptations followed. Most require medium heterogeneity to generate pressure gradients to enhance the relative flow of viscous fluids and increase dissipation. These include partial saturation (Norris 1993; Helle *et al.* 2003), fine layering (Gurevich *et al.* 1997; Gelinsky & Shapiro 1997; Pride *et al.* 2004), squirt-flow (Dvorkin & Nur 1993; Carcione & Quiroga-Goode 1996; Carcione *et al.* 2003, etc.). The question remains to determine whether it is necessary to introduce spatial inhomogeneities to get realistic attenuation.

Despite that de la Cruz and Spanos theory had remained controversial due to several impractical assumptions taken at the initial stages of its development (Pride *et al.* 1992), later changes were made in Hickey *et al.* (1995). Among them the inclusion of macroscopic shear modulus λ_M and fluid bulk viscosity ξ_f. The latter is

© 2007 The Authors
Journal compilation © 2007 RAS

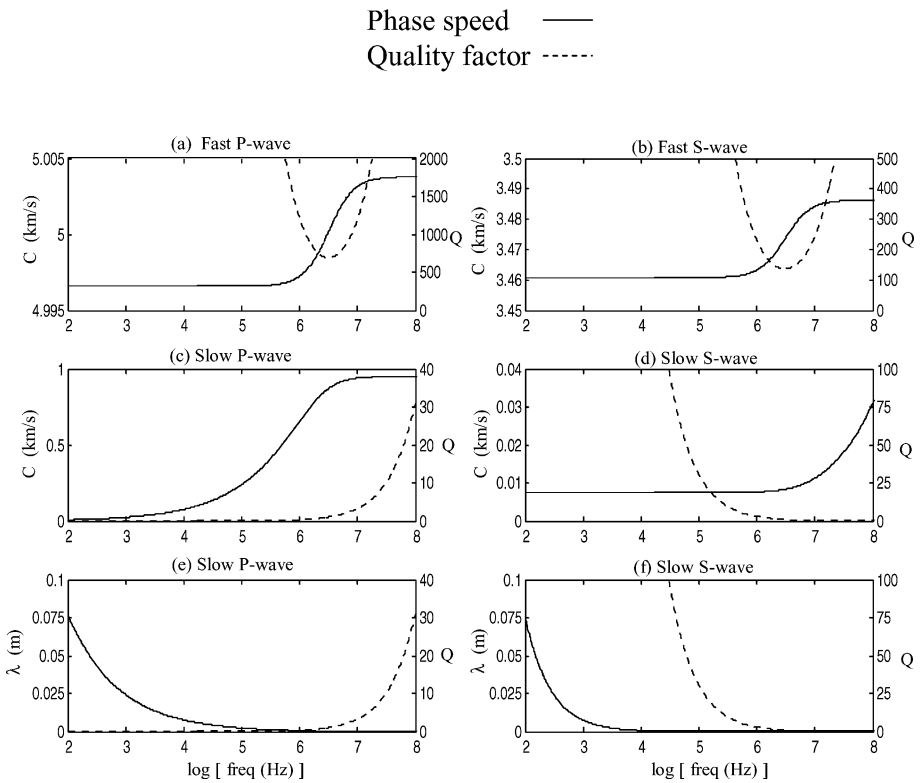


Figure 1. Attenuation and dispersion versus frequency for a water-saturated porous sandstone with $\eta = 0.05$ and $K = 3$ mD. The figure depicts the Quality factors (dash) and phase speeds (solid) of the fast *P* and *S* waves (a, b), of the slow *P* and *S* waves (c, d) and the corresponding wavelengths (e, f).

related to fluid shear viscosity μ_f by $\xi_f = \lambda_f + 2/3\mu_f$, where λ_f represents the second viscosity coefficient. Thus, for a spherically symmetric strain, the fluid bulk viscosity ξ_f is analogous to the bulk modulus of solids K, making λ_f and μ_f comparable to Lamé constants λ and μ. While dissipative studies of bulk viscosity in fluids ξ_f abound, its effects in porous materials has not been well documented, although it appears that it may make a significant contribution to the total loss (Pride *et al.* 1992).

The numerical results of Quiroga-Goode *et al.* (2005) confirm that Hickey's modifications to de la Cruz and Spanos theory (Hickey *et al.* 1995) produce waveforms that are remarkably similar to those of Biot. Nonetheless, that does not provide clear answers for what the sources of energy loss could be since Biot theory is known, among other things, for misrepresenting the magnitude and behaviour of attenuation and dispersion. Therefore, it was concluded in Quiroga-Goode *et al*. (2005), though only by inference, that the dynamic porosity in de la Cruz and Spanos theory (Hickey *et al.* 1995) may not have, ultimately, a strong nexus to dissipation. This is one of the issues to investigate in the present work.

While Biot and de la Cruz and Spanos theories, including that of Hickey, were developed in terms of solid and fluid deformations, they do not provide meaningful insight of the dynamics of porous media since field measurements must be related to the bulk deformations, as opposed to the separate individual constituents. To overcome this idealistic scenario, de la Cruz and Spanos equations were modified and reformulated by Sahay (1996) into a system whose field variables are now given in terms of the centre-of-mass and internal motions (as opposed to the individual solid and fluid motions). They are the fields which describe stretching as well as rotation (spinning) of material points in a poro-continuum (Sahay 1996). Just as in Hickey (1994), the system was derived within the framework of volume averaging and incorporates macroscopic shear modulus λ_M as a phenomenological parameter and fluid bulk viscosity ξ_f. It differs, among other things, in that thermomechanical coupling is neglected.

As can be noted from Sahay recast framework, the resulting formulation is largely analogous to phenomenological macroscopic theories that describe the dynamics of granular materials (see Bhattacharyya 1965 and references therein). In them, one of the vector equations represents the rotation of the grains about their centre of gravity, to account for intrinsic attenuation, while the second describes total linear momentum.

The most salient aspect of Sahay development is that it offers the simplest theoretical framework yet for analysing seismic wave propagation in porous isotropic isothermal media. Within this context, the Green's function were derived and synthetic waveforms computed in the ultrasonic regime, assuming the physical parameters of a rock sample similar to Berea sandstone, fully saturated with water (Sahay 2001). Although the amplitude and phase of the corresponding seismograms appear to show attenuation, it is not clear what portion can be ascribed to intrinsic dissipation, especially because no attenuation information is provided.

Therefore, to get a quantitative insight into that work another goal of this paper is to complement those results by computing amplitude attenuation, velocity dispersion and waveforms for that particular case and others.

This work is structured as follows. In the next section, the frequency domain wave equation of poroelasticity is outlined and expressions for phase velocity and quality factors obtained. After that, the kinematics of the wavefield is computed as a function of frequency, porosity and fluid viscosity for a siliciclastic rock similar to Berea sandstone. In the following section synthetic waveforms

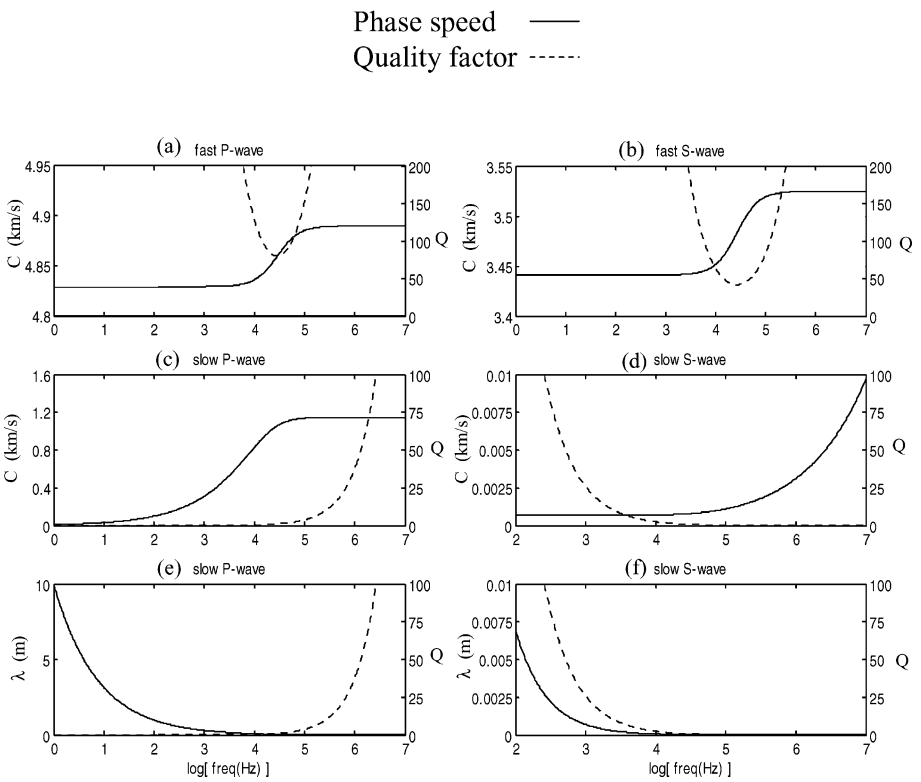


Figure 2. Attenuation and dispersion versus frequency similar to the previous figure except that porosity $\eta = 0.15$ and permeability $K = 700$ mD have increased.

are computed for those cases, focusing in the particular case in which attenuation is strongest. The conclusions are listed in the last section.

2 GOVERNING WAVE EQUATION

The reformulated theoretical background of Sahay (1996) describes the propagation of acoustic waves in porous media within the general framework of de la Cruz and Spanos theory. As it has been laid out in previous works only the most salient features are presented here. The theory predicts the propagation-diffusion of four waves in an unbounded homogeneous isotropic fully saturated porous medium. Two are similar to the classical *P* and *S* body waves propagating in single-phase elastic media. They are called fast waves. Strictly speaking, they are pseudo-longitudinal and pseudo-transversal waves, analogous to those propagating in viscoelastic media since particle polarization is not longer linear, that is, parallel or normal to propagation direction, but elliptical (Rasolofosaon 1991; Quiroga-Goode *et al.* 2006). The remaining two, which are referred to as slow waves, are diffusive; one is compressional and the other rotational. Thus both may be highly attenuated and dispersed depending on the frequency range and material properties. The fast waves are characterized by the solid and fluid moving in phase while the slow type represents out of phase motion. The slow *S* wave fails to appear in Biot theory as it neglects the viscous dissipation of momentum within the fluid.

The system of equations that prescribes linear deformations of fully saturated homogeneous isotropic porous rocks is, in the frequency domain (Sahay 1996):

$$\omega^2\mathbf{u}^{\mathrm{m}} + \alpha_{\mathrm{mm}}\nabla(\Delta\cdot\mathbf{u}^{\mathrm{m}}) - \beta_{\mathrm{mm}}\nabla\times\nabla\times\mathbf{u}^{\mathrm{m}} + \alpha_{\mathrm{mi}}\nabla(\nabla\cdot\mathbf{u}^{\mathrm{m}}) - \beta_{\mathrm{mi}}\nabla\times\nabla\times\mathbf{u}^{\mathrm{m}}, \tag{1}$$

$$\omega^2\mathbf{u}^{\mathrm{i}} + \alpha_{\mathrm{im}}\nabla(\Delta\cdot\mathbf{u}^{\mathrm{i}}) - \beta_{\mathrm{im}}\nabla\times\nabla\times\mathbf{u}^{\mathrm{i}} + \alpha_{\mathrm{ii}}\nabla(\nabla\cdot\mathbf{u}^{\mathrm{i}}) - \beta_{\mathrm{ii}}\nabla\times\nabla\times\mathbf{u}^{\mathrm{i}} = 0. \tag{2}$$

The first equation describes the total linear momentum of the porous medium, where $\mathbf{u}^{\mathrm{m}} = \mathbf{u}^{\mathrm{m}}(\mathbf{x},\omega)$ $(\mathbf{x} = x, y, z)$ represents the centre-of-mass field. It tracks volume fluctuations of the porous medium via dilatations and compressions. The centre-of-mass displacement of the porous medium is a dynamic quantity related to the individual motions of the solid matrix $\mathbf{u}_{\mathrm{s}}$ and the viscous fluids $\mathbf{u}_{\mathrm{f}}$ by

$$\mathbf{u}^{\mathrm{m}} = \frac{\rho_{\mathrm{s}}^{\mathrm{m}}\mathbf{u}_{\mathrm{s}} + \rho_{\mathrm{f}}^{\mathrm{m}}\mathbf{u}_{\mathrm{f}}}{\rho_{\mathrm{s}}^{\mathrm{m}} + \rho_{\mathrm{f}}^{\mathrm{m}}}, \tag{3}$$

where the individual solid and fluid masses are $\rho_{\mathrm{s}}^{\mathrm{m}} = (1-\eta)\rho_{\mathrm{s}}$ and $\rho_{\mathrm{f}}^{\mathrm{m}} = \eta\rho_{\mathrm{f}}$, respectively. Here, η represents porosity and ω to circular frequency. The solid and fluid densities correspond to ρ_{s} and ρ_{f}, respectively, and the mass-density of the porous continuum $\rho = \rho_{\mathrm{s}}^{\mathrm{m}} + \rho_{\mathrm{f}}^{\mathrm{m}}$.

In all previous works by de la Cruz and Spanos group, porosity η is defined as a dynamic variable to distinguish it from its static (constant) counterpart η_0 when the system is in equilibrium. As opposed to Biot theory, it appears explicitly in their system of equations with a corresponding Partial Differential Equation (PDE). However, after de la Cruz and Spanos equations were reformulated by Sahay (1996) the time-dependent porosity is no longer considered explicitly. Therefore, from here on η refers to the constant (static) porosity.

In porous media, a material point or representative volume element (RVE) tends to bifurcate as the solid $\rho_{\mathrm{s}}^{\mathrm{m}}$ and fluid masses $\rho_{\mathrm{f}}^{\mathrm{m}}$ follow separate trajectories, causing the material particle to spin around its own axis (Quiroga-Goode 2002a,b). That is the role played by $\mathbf{u}^{\mathrm{i}} = \mathbf{u}^{\mathrm{i}}(\mathbf{x},\omega)$ $(\mathbf{x} = x, y, z)$ in eq. (2) and it is how granular medium theories (Bhattacharyya 1965) empirically account for intrinsic attenuation. Therefore, the field $\mathbf{u}^{\mathrm{i}}$ characterizes the internal motion of the porous medium. This field, which is a measure of the spin of

© 2007 The Authors, *GJI*, **170,** 1227–1242
Journal compilation © 2007 RAS

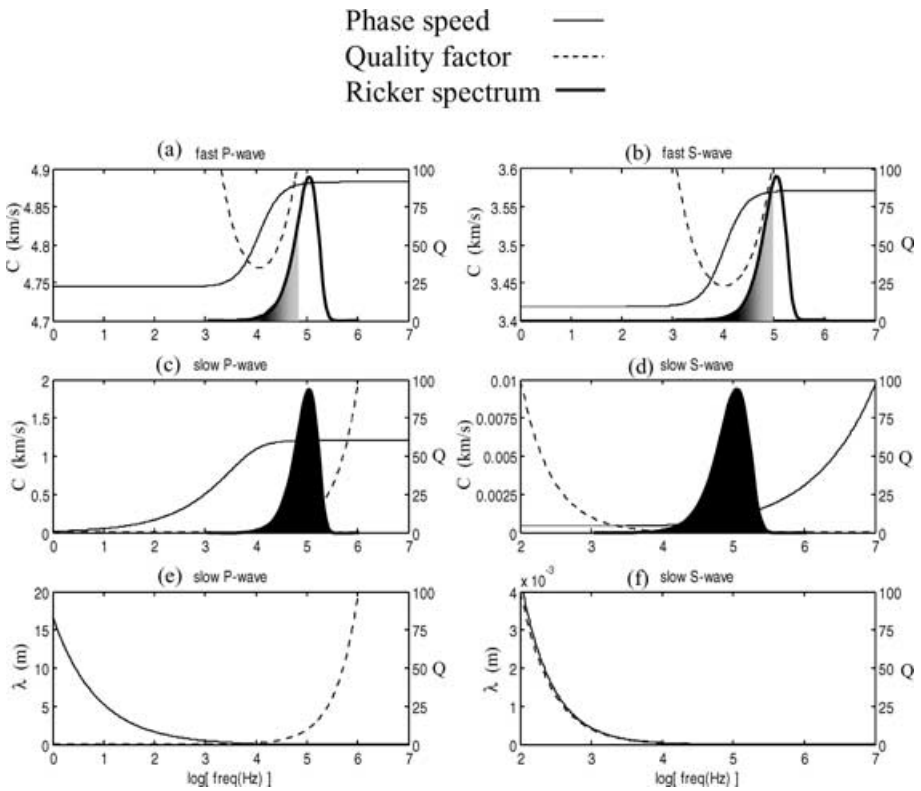


Figure 3. Attenuation and dispersion versus frequency similar to the previous figures except that porosity $\eta = 0.25$ and permeability $K = 3$ D have increased. The Ricker spectrum is superposed in (a–c) to show its relative position to the dissipation spectrum. The grey shades indicate the extent that intrinsic attenuation affects the fast and slow waves in Sahay (2001); darker means stronger.

the porous medium, is simply the differential motion between the solid matrix and the saturating fluid

$$\mathbf{u}_{\mathrm{i}} = \mathbf{u}_{\mathrm{s}} - \mathbf{u}_{\mathrm{f}}. \tag{4}$$

The coefficients α_{pq}'s and β_{pq}'s (p, $q = m$, i) in eqs. (1) and (2), which are dimensionally equal to complex velocity squares, correspond to the elements of the complex matrices:

$$\alpha = \begin{pmatrix} \alpha_{\mathrm{mm}} & \alpha_{\mathrm{mi}} \\ \alpha_{\mathrm{im}} & \alpha_{\mathrm{ii}} \end{pmatrix} \quad \text{and} \quad \beta = \begin{pmatrix} \beta_{\mathrm{mm}} & \beta_{\mathrm{mi}} \\ \beta_{\mathrm{im}} & \beta_{\mathrm{ii}} \end{pmatrix}. \tag{5}$$

They are given by

$$\alpha_{\mathrm{pq}} = \frac{1}{\rho^{\Omega}}\left[K_{\mathrm{pq}}^{\mathrm{Re}} + \frac{4}{3}\mu_{\mathrm{pq}}^{\mathrm{Re}} - i\omega\left(K_{\mathrm{pq}}^{\mathrm{Im}} + \frac{4}{3}\mu_{\mathrm{pq}}^{\mathrm{Im}}\right)\right], \tag{6}$$

and

$$\beta_{\mathrm{pq}} = \frac{1}{\rho^{\Omega}}\left(\mu_{\mathrm{pq}}^{\mathrm{Re}} - i\omega\mu_{\mathrm{pq}}^{\mathrm{Im}}\right), \tag{7}$$

where

$$\rho^{\Omega} = \begin{cases} \rho, & \mathrm{pq} = \mathrm{mm},\ \mathrm{mi} \\ \rho^{\mathrm{i}}\left(1 - \frac{i}{\omega\rho^{\mathrm{i}}}\delta_{\mathrm{v}}\right), & \mathrm{pq} = \mathrm{im},\ \mathrm{ii}. \end{cases} \tag{8–9}$$

The K's and μ's correspond to the physical parameters of the porous medium given in Appendix A for a siliciclastic type of rock. The superscripts Re and Im indicate the real and imaginary parts of the corresponding physical parameter and $i = (-1)^{1/2}$. The operator ∇ represents spatial differentiation. Density $\rho^{\mathrm{i}} = \rho^{r} - \rho^{12}$ is related to the reduced mass density $\rho^{r} = \rho_{\mathrm{s}}^{\mathrm{m}}\rho_{\mathrm{f}}^{\mathrm{m}}/\rho$. The parameter δ_{v} corresponds to the velocity-coupling coefficient. It is given by $-\mu_{\mathrm{f}}\,\eta^2/K$ where K represents the quasi-static permeability, which in the most general case should be frequency dependent, along with the bulk modulus of the matrix. The parameter ω^{i} has the dimension of frequency and corresponds to the Darcian relaxation central (peak) frequency, given by $-\delta_{\mathrm{v}}/\rho^{\mathrm{i}}$. The induced mass coefficient ρ^{12} measures the intercomponent force arising from the relative acceleration between the solid and fluid phases. It is taken to be $-\eta\rho_{\mathrm{f}}/3$.

Each of the 2×2 matrices eq. (5) has two complex eigenvalues λ_j^{α} and λ_j^{β} ($j =$ fast, slow) that result from the solution of the characteristic equation $\det(\boldsymbol{\alpha} - \lambda\mathbf{I}) = 0$ and $\det(\boldsymbol{\beta} - \lambda\mathbf{I}) = 0$, respectively, where $\mathbf{I}$ represents the identity matrix. Whenever α and β appear as super or subscripts, it means that they are related to compressional and shear deformations, respectively and refer to the wave type or wave type property. Two of those eigenvalues are related to diffusive phenomena, which give rise to the so-called P and S slow waves and two to propagation that are associated to the fast P and S waves.

It has been shown that a poroelastic rheology behaves effectively as a viscoelastic material since it is made up of an elastic solid frame and viscous fluids (Rasolofosaon 1991). In the strictest sense, the description of P and S waves propagating through multiphase or single-phase materials is simply reduced to the analysis of velocity dispersion and amplitude attenuation. In principle, viscoelasticity can encompass all types of dissipative phenomena described by single or two-component systems, provided that some of the predicted wave phenomena in the latter can be disregarded. Thus, the properties of homogeneous viscoelastic plane waves can be in principle extended to porous media.

The phase velocities and quality factors that characterize all four compressional and shear motions are thus related to the eigenvalues of eq. (5) by

$$C_j^{\psi} = \frac{1}{\mathrm{Re}\left[1/\left(\lambda_j^{\psi}\right)^{1/2}\right]}, \tag{10}$$

© 2007 The Authors, *GJI*, **170,** 1227–1242
Journal compilation © 2007 RAS

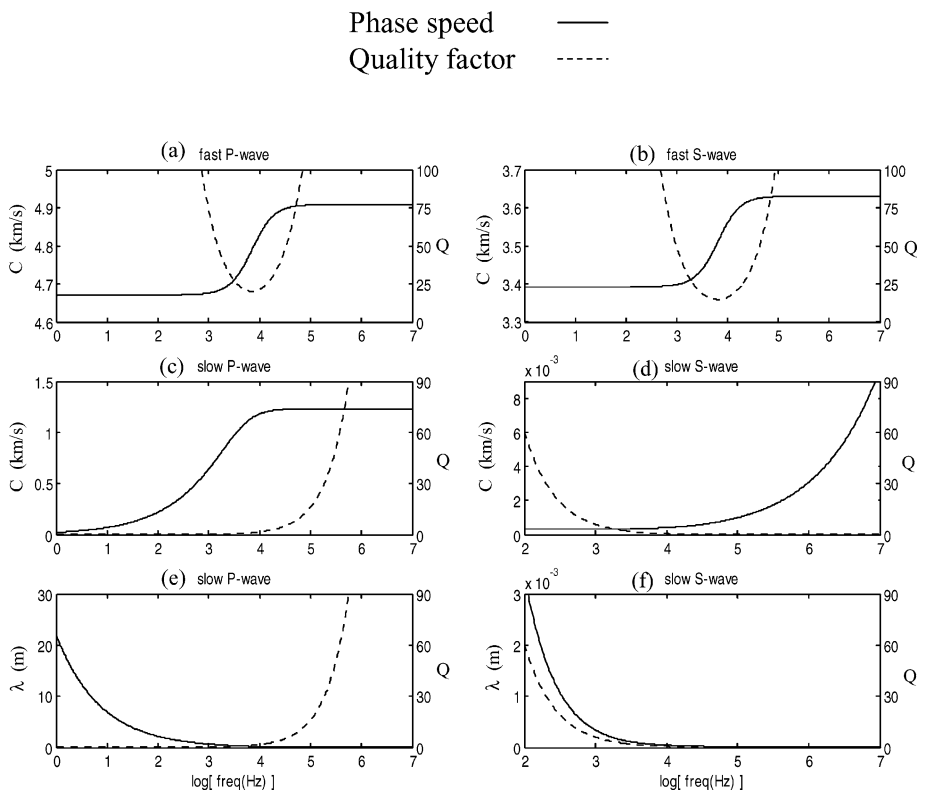


Figure 4. Attenuation and dispersion versus frequency similar to the previous figures except that porosity and permeability have increased further ($\eta = 0.35$ and $K = 7$ D). As porosity increases to 0.35, the seismic waves will experience the largest losses.

and

$$Q_j^{\psi} = \frac{\mathrm{Re}\left(\lambda_j^{\psi}\right)}{\mathrm{Im}\left(\lambda_j^{\psi}\right)}, \tag{11}$$

respectively, where $\psi = \alpha, \beta$ and $j =$ fast, slow. Re and Im take on the real and imaginary parts of the complex eigenvalues. As Biot theory does not consider intrinsic dissipation within the viscous fluid, the slow S wave does not appear in his equations.

It should be kept in mind that since the phase speeds C_j^{ψ} are derived for homogeneous P and S plane waves, their magnitudes are greater than those of the inhomogeneous counterparts (Borcherdt 1973). Similarly, the maximum attenuation of the homogeneous waves (minimum Q_j^{ψ}) is less than that of the corresponding inhomogeneous equivalent. Numerical examples of velocity dispersion and attenuation for a sandstone are presented in the next section.

3 DISSIPATIVE PROPERTIES OF BEREA SANDSTONE

It is computed the dissipative properties as a function of frequency using eqs. (10) and (11) for the same type of siliciclastic rock as that of Sahay (2001). Furthermore, additional cases are also computed to consider varying porosity, permeability and saturate type.

The complex eigenvalues are simply computed with

$$\lambda_j^{\psi} = \frac{\mathrm{tr}(\mathbf{A}) \pm \sqrt{\mathrm{tr}(\mathbf{A})^2 - 4\Delta_{\mathrm{A}}}}{2}, \tag{12}$$

where matrix $\mathbf{A}$ refers to matrices $\boldsymbol{\alpha}$ and $\boldsymbol{\beta}$ given in eq. (5). Here tr and Δ represent the trace and determinant, respectively. The elements of the preceding matrices are computed with expressions (6)–(9), given the corresponding moduli in Appendix A whose petrophysical parameters are found in Appendix B.

De la Cruz and Spanos equations were developed under the assumption that the compressible flow of fluids obeys the Navier–Stokes equation. Nonetheless, it has been customary in the literature to assume the flow laminar, such that for frequencies above the Poiseuille limit and for cylinder-like pore geometries

$$f^P = \frac{\eta \mu_{\mathrm{f}}}{2\pi \rho_{\mathrm{f}} K} \tag{13}$$

the limit breaks down. Parameter K represents permeability. This upper bound for a Berea type of sandstone corresponds to $f^P \sim 3.6$ GHz, taking the shear viscosity of oil and the smallest pore space and permeability (Appendix A). As will be seen ahead, some unrealistic numerical results are obtained close to this limit, which suggests that the limit (13) may be too high.

3.1 Attenuation versus porosity

The strength of seismic attenuation can be assessed in terms of amplitude attenuation and velocity dispersion. Figs 1(a)–(d) display the phase speeds and quality factors Q of the fast compressional and shear waves versus frequency for the typical case when the porous medium is fully saturated with water. It is first considered the case of $\eta = 0.05$ and $K = 0.002$ Darcy (2 mD).

The relaxation peak is centred approximately at 3 MHz ($10^{6.5}$ in the log scale). Due to the small amount of fluids (low porosity), the fast P and S waves exhibit little attenuation (Figs 1a and b), that is, $Q^{\alpha}_{\mathrm{fast}} \approx 750$ and $Q^{\beta}_{\mathrm{fast}} \approx 150$. The slow P wave, shown in Fig. 1(c), starts to reach a sizeable speed of almost 1 km s^{-1} approximately after 10 MHz but cannot propagate due to its high attenuation, that

© 2007 The Authors, *GJI*, **170,** 1227–1242
Journal compilation © 2007 RAS

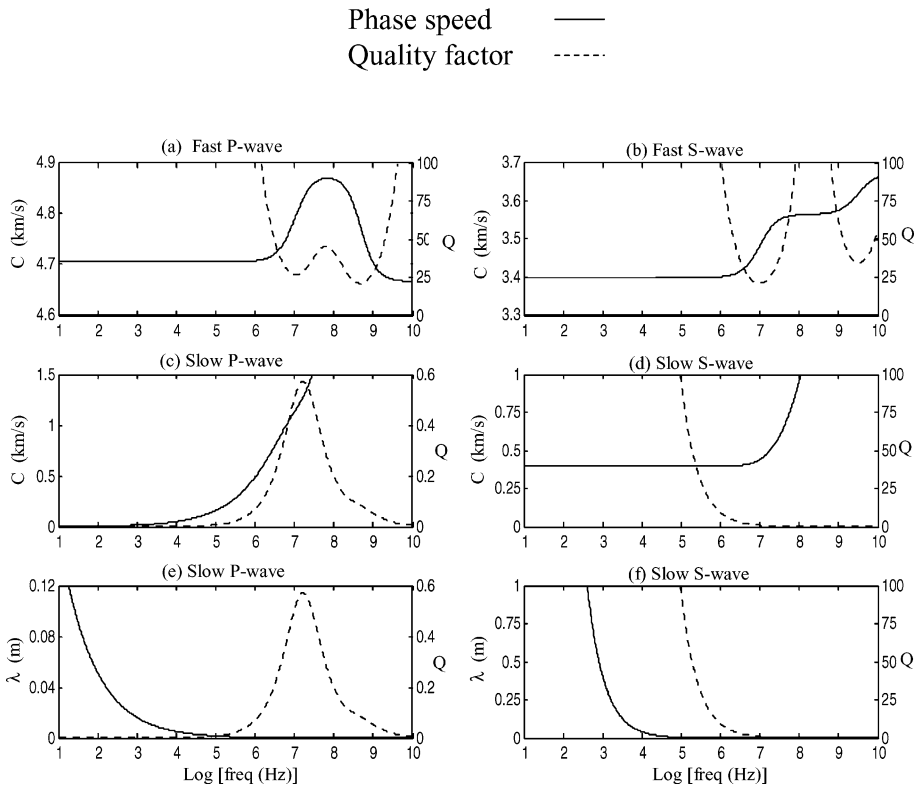


Figure 5. Attenuation and dispersion versus frequency similar to Fig. 3 except that water has been substituted with oil ($\eta = 0.25$ and $K = 3$ D). No physical significance may be attributed to the appearance of the relaxation spectrum at high frequency since it is beyond Poiseuille frequency limit.

is, $Q^{\alpha}_{\rm slow} \approx 20$ (below 100 MHz). Although there is a narrow window within which it could become propagative at 32 MHz, where $Q^{\alpha}_{\rm slow} \approx 70$, Fig. 1(e) shows that the corresponding wavelengths are very small to hold physical significance.

The slow *S* wave on the other hand (Fig. 1d) displays an opposite behaviour as its slow *P* equivalent. That is, as the frequency decreases, the quality factor increases rapidly to ∞, implying that it could propagate largely unattenuated within this frequency range, that is, $<$31 kHz. However it would do so at very low speeds (10 m s^{-1}). As will be seen further below, the computed wave amplitudes are so small that, from the theoretical point of view, the wave is practically non-existent.

Fig. 2 shows that as porosity and permeability are increased, the relaxation peak shifts towards lower frequencies. It is observed that increasing the pore space causes the attenuation and dispersion of the fast *P* and *S* waves to grow substantially, that is, approximately by two orders of magnitude. The quality factors correspond to $Q^{\alpha}_{\rm fast} \approx 62$ and $Q^{\beta}_{\rm fast} \approx 40$, respectively, while dispersion has risen. The slow *P*-wave phase speed increases asymptotically to a constant value of almost 1.2 km s^{-1} after 100 kHz, although it could become propagatory after 1.5 MHz. The phase speed of the slow *S* wave on the other hand, has slowed down and the low frequency band in which the wave could become propagatory has been reduced, precluding all possibility to travel.

Fig. 3 depicts the wave properties for the 25 per cent porosity sandstone fully saturated with water, which would correspond to the synthetic seismograms computed in Sahay (2001). The wavefield calculated in that work (Figs 1–4) focuses only onto the ultrasonic regime, which simulates a laboratory setting. Despite the evident reduction in amplitudes with increasing distance (from 0.1 to 1 m), which was illustrated in those figures for the fast *P* and *S* waves, and the slow *P* wave, no amplitude analysis was provided to quantify to what extent the attenuation shown in the synthetics was directly related to intrinsic loss. From those figures it can be seen that of all three waves, the slow *P* wave undergoes the highest amplitude drop. No trace of the slow *S* wave can be seen, as expected.

The spectrum of the Ricker wavelet used to calculate the synthetic signals in Sahay (2001), whose dominant frequency corresponds to 100 kHz, has been added in Fig. 3 (thick solid line). Its shape does not appear symmetrical since it has been plotted in log scale to match the frequency axis of the dispersion and quality factors. Although the units of the pulse spectrum do not correspond to those of the phase speed or Q, which is non-dimensional, it clearly shows that the relaxation curves (quality factors) of the fast *P* and *S* waves are slightly off to the side of the source peak band. The grey shades within the source spectrum indicate the portion most affected by attenuation; darker implies stronger energy damping. Figs 3(a) and (b) indicate that the fast *P* and *S* waves in Sahay (2001) should not be substantially affected by intrinsic attenuation, as it had been the case if the source and the relaxation spectra were overlapped. Nevertheless, the lower frequency portion of their spectra must undergo some attenuation, more so the fast *S* wave since $Q^{\beta}_{\rm fast} \approx 25$ at 10 kHz. It can also be seen in Figs 3(c) and (d) that it is the slow *P* and *S* waves the ones that would experience the strongest amplitude attenuation and dispersion, confirming thus the results of Sahay (2001).

It can be noted that given the width of the dissipation spectrum, $Q^{\alpha}_{\rm fast}$ and $Q^{\beta}_{\rm fast}$ vary only by 25 per cent, making the Q's nearly constant within this source frequency band.

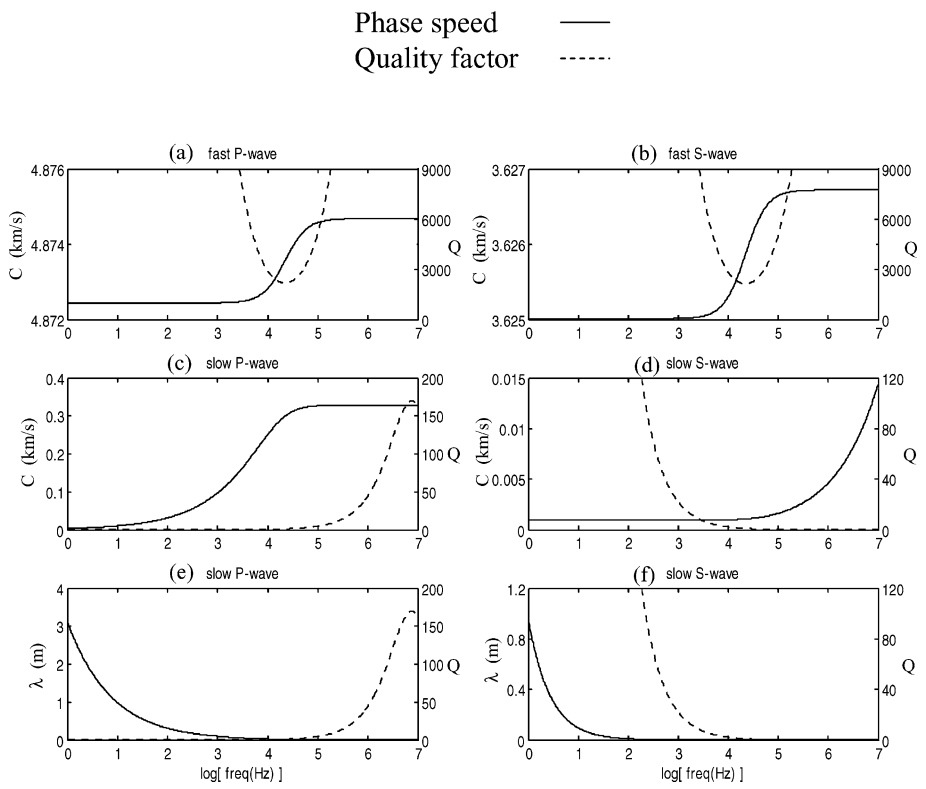


Figure 6. Attenuation and dispersion versus frequency similar to previous figures except that gas has replaced water in the porous sandstone with $\eta = 0.25$ and $K = 3$ D.

As the amount of fluids saturating the porous media is increased (increasing porosity to 35 per cent in Fig. 4), velocity dispersion of the fast *P* and *S* waves jumps to 5 and 8 per cent, respectively, and attenuation changes to $Q^{\beta}_{\text{fast}} \approx 20$ and $Q^{\beta}_{\text{fast}} \approx 12$.

The wavelengths of the slow *P* wave are slightly enhanced, and so are its phase speeds. Furthermore, the frequency window in which the slow *S* wave could propagate is reduced because the relaxation mechanism expands towards lower frequencies. The phase speed for this wave remains extremely low when water is permeating the porous medium. This condition will change as other fluids are considered.

3.2 Attenuation versus fluid viscosity

The dissipative properties of the sandstone are shown in Fig. 5 when it is fully saturated with oil. Although the case of increasing porosity has been examined when oil is permeating the porous medium, it is only shown here the numerical results for the more interesting case of higher porosity ($\eta = 25$ per cent). As can be observed in Figs 5(a) and (b), the wide relaxation mechanism that would be seen for low porosity ($\eta < 5$ per cent) oil saturated rock, or from the preceding cases of water saturated porous medium (Figs 1–4), has split into two distinct narrow mechanisms. This is clearly observed in the fast rotational wave.

The first relaxation mechanism, whose peak is located at

$$\omega^{\text{i}} = -\frac{\eta^2 \mu_{\text{f}}}{K(\rho^r - \delta^a)} \tag{14}$$

is centred at approximately 20 MHz, which corresponds to $10^{7.3}$ in the log scale. Their magnitude is $Q^{\alpha}_{\text{fast}} \approx 27$ and $Q^{\beta}_{\text{fast}} \approx 18$, respectively. The second relaxation peak is centred at 400 MHz for the fast *P* wave, whereas for the fast *S* wave, it is located approximately at 3 GHz. It should be pointed out that it is stronger for the fast *P* wave ($Q^{\alpha}_{\text{fast}} \approx 18$) than its shear counterpart ($Q^{\beta}_{\text{fast}} \approx 30$). The Poiseuille frequency limit in this case is either 12.2 or 122 MHz, depending of whether the oil viscosity is taken as shear or bulk, respectively. However, not much physical significance can be drawn from the results at high frequencies, unless a stricter analysis of the Poiseuille limit is developed. Nevertheless, in this frequency range the seismic wavelengths are reaching the grain size, which would cause scattering not considered in the theory.

In the case of the slow *P* wave, the quality factor as a function of frequency displays a peak at approximately 10 MHz and the phase speed increases unrealistically beyond 10 MHz. Even in the case that this was physically plausible, the extremely high attenuation ($Q^{\alpha}_{\text{slow}} < 1$) would preclude the wave from propagating. The slow *S* wave also displays unrealistic dispersion behaviour as the phase speed grows substantially after 10 MHz.

In the low frequency range (<100 kHz), the slow *S* wave reaches constant low speed of almost 400 m s^{-1} (Fig. 5d), in the region where attenuation is negligible ($Q \to \infty$). It resembles as if a low porosity rock were saturated with water (Fig. 1c), except for one notable feature: the slow *S* wave speed has increased two orders of magnitude within this band. In principle, this would seem to indicate that the slow shear wave could become propagatory. The computation of synthetic seismograms shown in the next section will confirm that from the theoretical point of view, the slow *S* wave does not propagate.

The effect of decreasing fluid viscosity, that is, when gas is fully saturating the porous medium, is that the fast *P* and *S* waves propagate unattenuated since *Q* values are above 3000 (Fig. 6). There is practically no dispersion. The slow *P* wave could propagate at high

© 2007 The Authors, *GJI*, **170,** 1227–1242
Journal compilation © 2007 RAS

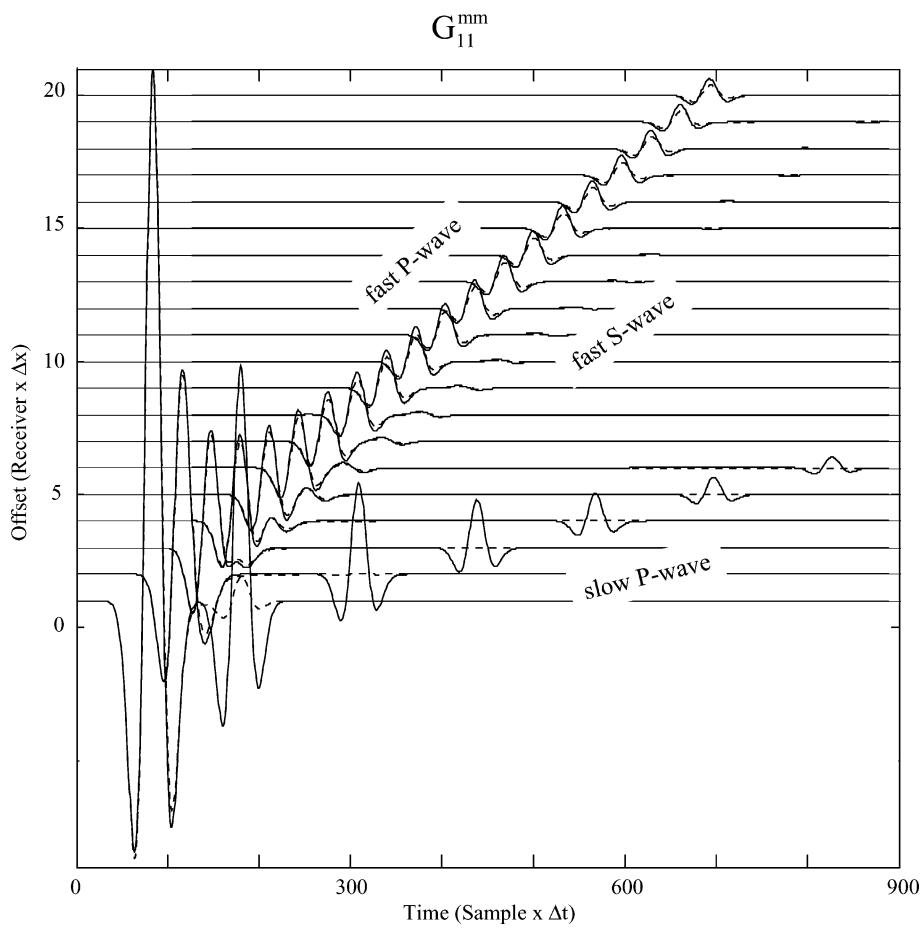


Figure 7. Synthetics computed using the Green's function G_{11}^{mm} versus distance for a water-saturated porous medium with $\eta = 0.25$. It compares the dissipation effects of changing the source dominant frequency from $f_0 = 100$ kHz (as in Sahay 2001) to 10 kHz. The units of the coordinate axis depend on the source peak frequency, as indicated in the plot.

frequencies (>8 MHz) but with low phase speeds. For frequencies below 10 Hz, the slow S wave shows a constant low velocity of 1 m s^{-1}.

The next section presents the computation of synthetic seismograms considering a porous siliciclastic rock similar to that of Sahay (2001).

4 SYNTHETIC WAVEFORMS

To complement the computational results of Sahay (2001), the goal of this section is to investigate the dispersion and attenuation effects of varying porosity, fluid viscosity and source frequency band on the propagation of seismic waves. Special attention is focused to determine the extent that the amplitude attenuation of the synthetic seismograms depicted in that work is related to intrinsic dissipation.

The derivation of the Green's function can be found in Sahay (2001) and will not be repeated. Each of the four waves ($n = 1, 4$) predicted by theory is computed with:

$$G_{jk}^{pq}(\mathbf{x},\omega) = \sum_{n=1}^{4}\left[A_n^{pq}(\omega)\partial_j\partial_k + B_n^{pq}(\omega)\delta_{jk}\right]\frac{e^{i\omega s_n r}}{4\pi r}, \tag{15}$$

where $(p, q = m, i)$, $(j, k = 1, 3)$ and

$$A_n^{pq}(\omega) = \frac{1}{\omega^2}\left[(-1)^n\frac{(\alpha^{\dagger})^{pq}}{\Delta_\alpha}\frac{\delta_{1n}+\delta_{2n}}{s_1^2-s_2^2} - (-1)^n\frac{(\beta^{\dagger})^{pq}}{\Delta_\beta}\frac{\delta_{3n}+\delta_{4n}}{s_3^2-s_4^2} - \delta_{pq}\frac{\frac{1}{\Delta_\alpha}\left(s_n^2-s_3^2-s_4^2\right)-\frac{1}{\Delta_\beta}\left(s_n^2-s_1^2-s_2^2\right)}{\left(s_{n+3}^2-s_n^2\right)\left(s_{n+2}^2-s_n^2\right)\left(s_{n+1}^2-s_n^2\right)}\right] \tag{16}$$

and

$$B_n^{pq}(\omega) = (-1)^n\frac{1}{\Delta_\beta}\left[\delta_{pq}-(\beta^{\dagger})^{pq}s_n^2\right]\frac{\delta_{3n}+\delta_{4n}}{s_3^2-s_4^2}, \tag{17}$$

where s_n^2 corresponds to the reciprocals of the complex eigenvalues λ_j^{ψ} (eq. 12), Δ_α and Δ_β to the determinants of the 2 × 2 complex velocity matrices (eq. 5) related to the compressional and shear waves and δ_{jk} (=1 for $j = k$, $p = q$; or 0 for $j \neq k$, $p \neq q$), correspond to the delta function. The symbol † denotes determinant weighted inverse matrix (and matrix element). Using the identity

$$\partial_j\partial_k\left(\frac{e^{i\omega s_n r}}{4\pi r}\right) = \omega^2\frac{e^{i\omega s_n r}}{4\pi r}\left[\frac{i\omega s_n r-1}{\omega^2 r^2}\left(\delta_{jk}-3\gamma_j\gamma_k\right)-\gamma_j\gamma_k s_n\right], \tag{18}$$

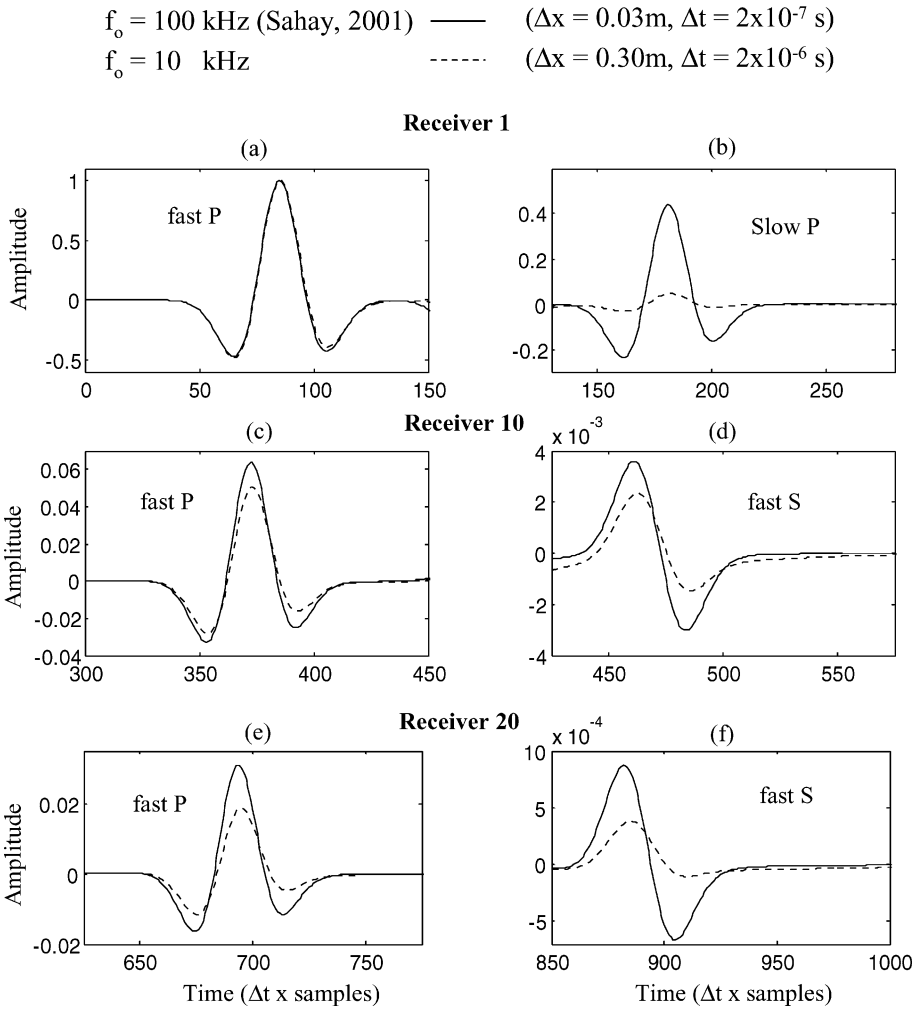


Figure 8. Three traces extracted from previous Fig. 7. Each seismogram is divided into two time windows and scaled. Plots (a, b) correspond to the receiver 1, plots (c, d) to receiver 10 and (e, f) to receiver 20. It can be observed in plots (c, d) that the fast *S*-wave attenuation is stronger than its compressional counterpart.

where $\gamma_j = x_j/r$ represent the direction cosines and $s_n = s_n^+ + is_n^-$ are the complex slownesses

$$s_n^+ = \sqrt{\frac{1}{2}\left(\sqrt{\mathrm{Re}\left(s_n^2\right)^2 + \mathrm{Im}\left(s_n^2\right)^2} + \mathrm{Re}\left(s_n^2\right)^2\right)} \tag{19}$$

$$s_n^- = \sqrt{\frac{1}{2}\left(\sqrt{\mathrm{Re}\left(s_n^2\right)^2 + \mathrm{Im}\left(s_n^2\right)^2} - \mathrm{Re}\left(s_n^2\right)^2\right)} \tag{20}$$

It should be noted a typographical error in the Green's function of Sahay (2001, eq. 40): the factor $(\beta^{pq})^{2\dagger}$ should be $(\beta^{\dagger})^{pq}$ (Sahay, private communication, 2006). That term is within the square brackets in this work (eq. 17). The Green's function is then used to compute the synthetic seismograms in the frequency domain and converted to time via a fast Fourier transform algorithm. Similar to Sahay's work, the temporal function of the source corresponds to the Ricker wavelet. The spectrum is depicted in Fig. 3 for a dominant frequency of $f_0 = 100$ kHz (as in Sahay 2001). The physical parameters of the fluid saturated porous rock can be found in Appendix B.

The effects of two kinds of sources are examined and two types of variables recorded: centre-of-mass and internal field. In the first kind of source, the excitation is applied to the bulk of the porous material such that the solid matrix and the viscous fluids experience the same acceleration. The second kind of excitation is a fluid injection in which a force (per unit mass) acts only into the fluid phase. Therefore, from here on, the seismic wavefields are to be identified as G_{jk}^{pq} (p, $q = m$, i; j, $k = 1, 3$), where (sub) superscripts refer to the 'p' type of displacement field in the jth direction due to the excitation of the 'q' kind of source in the kth direction.

4.1 Source frequency band versus relaxation spectrum

The equations of motion are constructed under the assumption that the smallest seismic wavelength be greater than the RVE, so that a continuum description is firmly established. Therefore, from volume averaging: $a \ll l \ll \lambda_{\min}$, where a represents the average grain size, l stands for the length of RVE and $\lambda_{\min}$ is the minimum wavelength. Taking Berea average grain size $a = 100$ μm, thus $\lambda_{\min} = 1$ mm. Therefore, assuming the maximum phase speed of 5 km s^{-1} (fast P wave), the high frequency limit that will meet the requirement of previous inequality should be 5 MHz.

As shown in the foregoing section, the dissipative behaviour in Fig. 3(a) and (b) reveals that the fast and P waves computed in Sahay

© 2007 The Authors, *GJI*, **170,** 1227–1242
Journal compilation © 2007 RAS

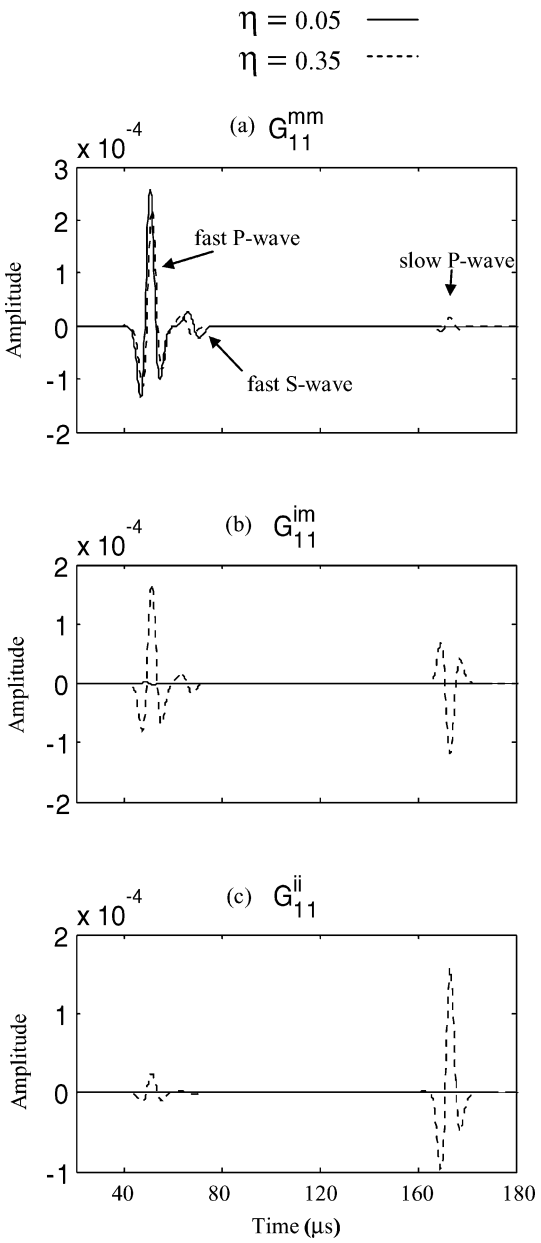


Figure 9. Synthetics computed for (a) G_{11}^{mm}, (b) G_{11}^{im} and (c) G_{11}^{ii} for a water-saturated porous medium with $f_0 = 100$ kHz. It compares the dissipation effects of different porosities. Source–receiver distance is 0.2 m. For $\eta = 0.05$ (solid line) the source and dissipation spectra are fully separated, while for $\eta = 0.35$ the relaxation spectrum is overlapped by the low frequency components of the source spectrum.

(2001) for a sandstone fully saturated with water were not substantially affected by intrinsic attenuation and dispersion since the most energetic portion of the source frequency band does not overlap the relaxation spectrum fully. Therefore, given the source dominant frequency ($f_0 = 100$ kHz) and the physical parameters of the porous medium with $\eta = 0.25$, it is inferred that the amplitude decrease with travelled distance in Sahay (2001) is partly a geometrical spreading effect.

This is confirmed in Fig. 7, which compares two sets of synthetic seismograms. The first was obtained for a source dominant frequency of 100 kHz (solid line). In this case the source and the relaxation spectra are slightly offset from each other (Sahay 2001). The second is for $f_0 = 10$ kHz (dash line). In this case both spectra overlap and thus attenuation is the strongest. The various types of seismic waves are identified in the plot, including the slow P wave, which becomes propagatory within this frequency band. It undergoes stronger attenuation than the fast waves, decaying more rapidly with distance. Its amplitudes are substantially smaller for $f_0 = 10$ kHz and thus cannot be observed at this scale (see Fig. 3). The source is similar to the type used in land exploration where the excitation is applied to the bulk of the porous material. The recorded theoretical wavefields correspond to the centre of mass (G_{11}^{mm}), which is quantity related to what would be recorded from geophones. Therefore, it is by centring the source frequency band within the relaxation spectrum that the full dissipation effects are induced on the propagation of seismic waves, within the frequency range predicted by the relaxation phenomena.

Due to the difference in frequencies between the two sets of seismograms, the waveforms would have been wider for $f_0 = 10$ kHz. Thus, to make possible the comparisons between the two frequency bands, the receiver locations were set farther apart such that the seismic waves travelled exactly the same number of wavelengths with 10 kHz as with 100 kHz. The time and offset axis are scaled in Fig. 7 by the corresponding Δx and Δt factors, as indicated in the plots. The synthetic waveforms are scaled such that the amplitudes of the fast P waves (with 10 and 100 kHz) in the first trace (smallest offset) are the same.

Fig. 8 shows a close-up of the synthetic signals in Fig. 7 from receivers 1 (a and b), 10 (c and d) and 20 (e and f). The timescale has been preserved in all these plots (a–e) to assess the extent that the waveforms have spread out due to attenuation and dispersion. The rate of decay of the slow P wave is higher than the fast S and P waves. Additionally, the fast S wave is dissipated more rapidly than its compressional counterpart.

4.2 Porosity effects versus source type

To compare the effects of intrinsic loss with varying porosity ($\eta = 0.05$ and 0.35), for the two types of sources (centre of mass and fluid injection) and the two kinds of natural vibrations (centre of mass and internal fields), it is depicted in Fig. 9 the synthetic seismograms for a series of receivers, considering an excitation with $f_0 = 100$ kHz. The quantity G_{11}^{mm} corresponds to the centre-of-field displacement (m) measured along direction 1 (x-axis) due to the centre-of-field excitation (m) exerted in direction 1 (x-axis).

In the remaining two plots (Figs 9b and c), G_{11}^{im} and G_{11}^{ii} both represent the recorded internal field, but the first is actuated by a centre-of-mass excitation and the second by a fluid injection, respectively. The various types of recorded seismic waves are identified in Fig. 7(a).

It can be seen in Fig. 9 that as porosity is increased from 5 to 35 per cent, the fast P wave is delayed and its amplitudes diminished as expected due to the softening of the effective bulk modulus of the rock. The fast S wave propagates faster with increasing porosity (compare phase speeds in Figs 1b and 4b), causing it to arrive earlier. This result appears in principle counterintuitive since the bulk shear modulus should be expected to decrease as more fluids are incorporated into the porous rock.

Except for the amplitude reduction due to spherical divergence, the fast P and S waves travel largely unattenuated for $\eta = 0.05$ since, as analysed previously (Figs 1a and b), the source band with $f_0 = 100$ kHz, which is where $Q \to \infty$, and the dissipation spectrum (with $\omega^i = 3$ MHz), are separated by more than two decades (log).

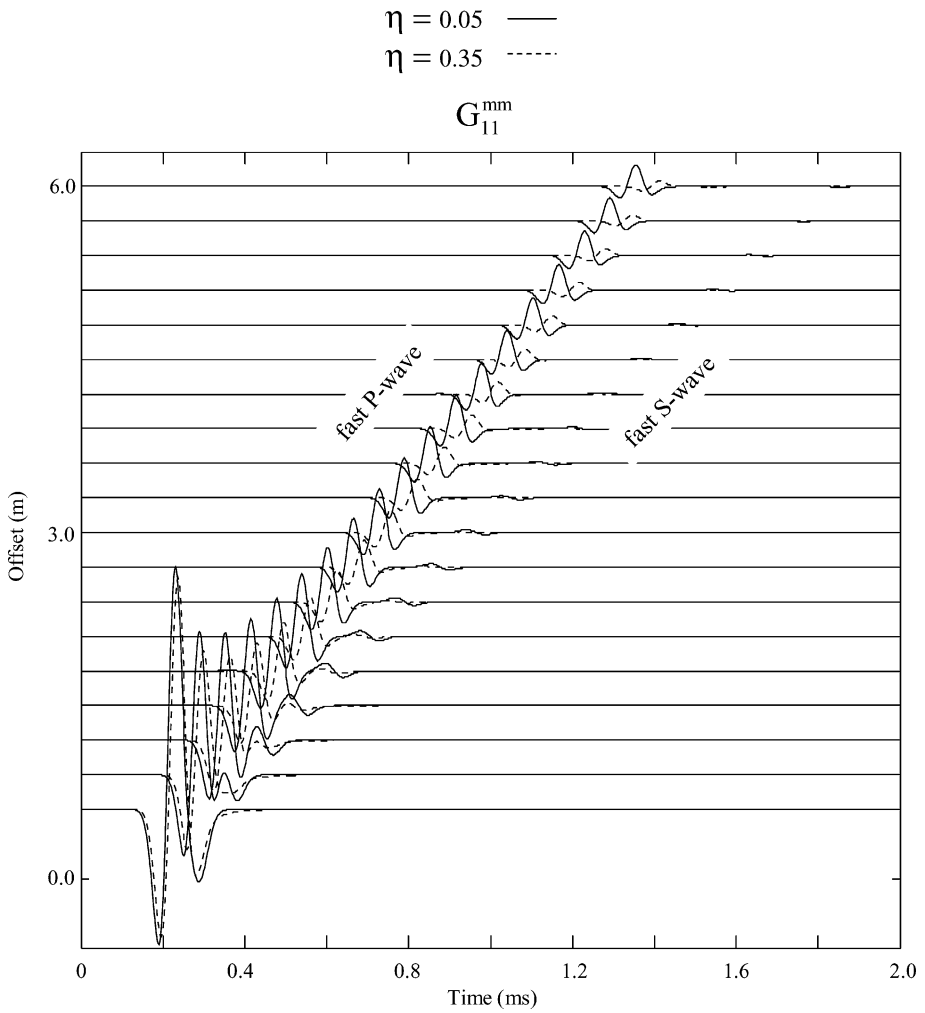


Figure 10. Synthetics computed analytically for G_{11}^{mm} versus distance for a water-saturated porous medium with different porosity and $f_0 = 10$ kHz. By shifting the source dominant frequency down a decade (log), the source and dissipation spectra overlap fully, inducing maximum attenuation.

For $\eta = 0.35$, the relaxation spectrum, with $\omega^i = 10$ kHz, slightly overlaps the lower frequency components of the fast *P* and *S* waves. Thus they should experience some dissipation (although little dispersion). By inference, it can be deduced that in this case, it is experienced stronger attenuation than the case of Sahay (with $\eta = 0.25$) because even though the relaxation peak has slightly shifted toward lower frequencies, the *Q*'s are smaller, implying thus higher dissipation. The high frequencies above the dominant ($\geq$100 kHz) propagate largely without loss as Q^{α}_{fast} and $Q^{\beta}_{\text{fast}} \to \infty$ within that band.

The slow *P* wave is activated as the amount of fluids increases, as observed in Fig. 9, since it results from the shearing of fluids relative to the porous matrix. Its phase speed increases and attenuation diminishes with increasing porosity (compare Figs 1c and 4c). The slow *S* wave is strongly diffusive, as can be judged from Figs 1(d) and 4(d). Contrary to the slow *P* wave, its phase speed grows with decreasing porosity and Q^{β}_{slow} increases with decreasing frequency. For instance, for $\eta = 0.05$, the phase speed is constant at 10 m s^{-1} and $Q^{\beta}_{\text{slow}} > 100$ within the lower portion of the source spectrum, but the range of wavelengths that could propagate fades to zero within that frequency band. Thus, it does not appear in any of the synthetics, regardless of the type of source or the kind of recorded wavefield.

Applying a fluid injection to the porous medium (Fig. 9b) causes the amplitudes of both compressional waves (fast and slow) to be boosted with increasing porosity. As can be seen in this figure, the amplitude of the slow *P* wave is about the same magnitude of its fast counterpart, but gets even larger if measured in the internal field (Fig. 8c).

Fig. 10 depicts the synthetic seismograms with varying porosity (0.05 and 0.35) and increasing distance (up to 6 m). In this case, the dominant frequency was shifted down to 10 kHz, as opposed to the previous case (Fig. 9) in which $f_0 = 100$ kHz. The dissipation mechanism and the source spectra overlap fully for $\eta = 0.35$ but are far apart for $\eta = 0.05$. The main outcome is that while for low porosity the fast *P* and *S* waves travel mostly unattenuated, except for the amplitude decrease associated to the divergence of the wavefront, they experience strong attenuation with higher porosity as expected, due to the highest amplitude attenuation and dispersion possible ($Q^{\alpha}_{\text{fast}} = 18$ and $Q^{\beta}_{\text{fast}} = 13$). Therefore, the initial waveform of the Ricker time function has been substantially modified.

This can be observed better in Figs 11(a), (c) and (e) where it is depicted the waveforms for receiver 20, which is located at 6 m from the source location. For comparison, the fast *P* and *S* waves are shown for $f_0 = 100$ kHz in Figs 11(b), (d) and (f). Note that in both cases, the waves have propagated the same number of wavelengths

© 2007 The Authors, *GJI*, **170,** 1227–1242
Journal compilation © 2007 RAS

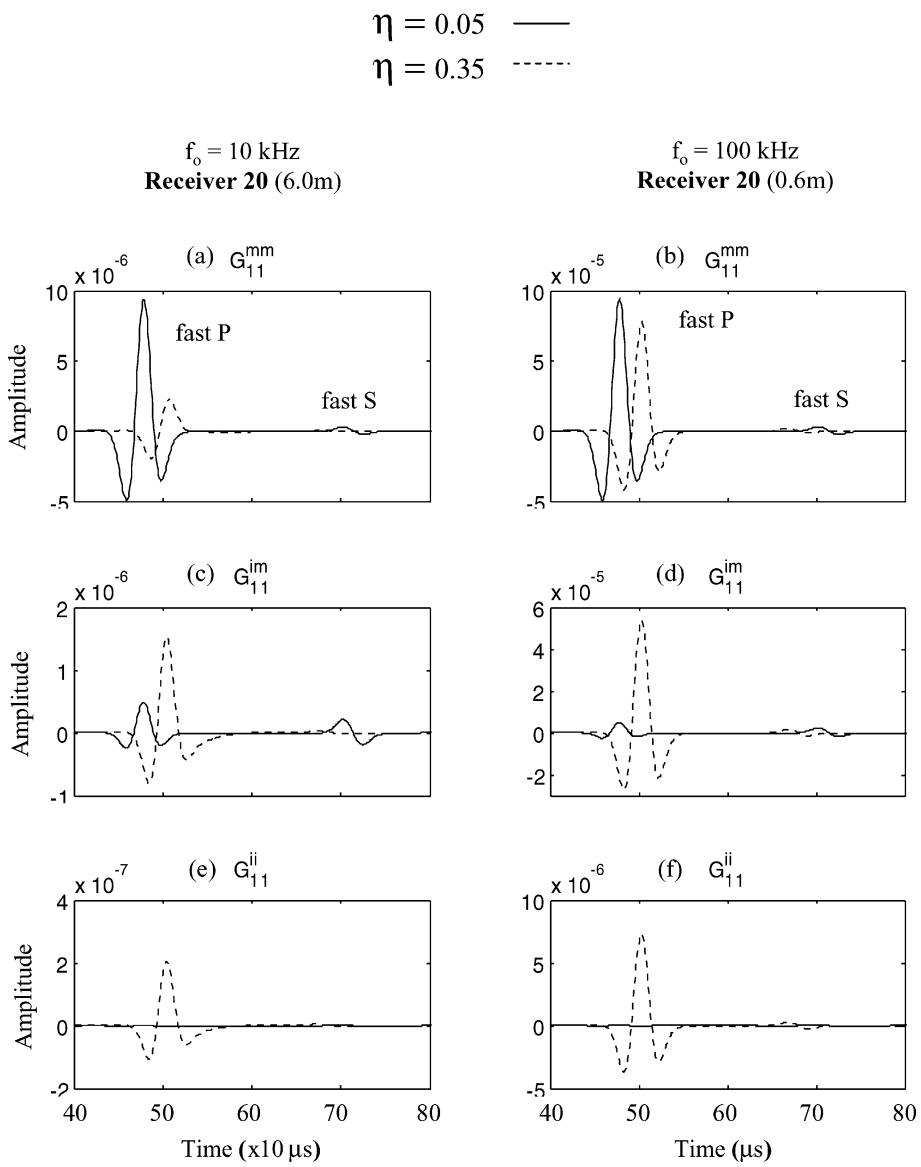


Figure 11. A synthetic trace (plots a,c and e) extracted from previous Fig. 10 (with $f_0 = 100$ kHz) and compared to the case whose source peak frequency is 100 kHz (plots b, d and f). The timescale in plots (a, c and e) has been shrunk to make the comparison with (b, d and f) possible.

and that the only difference is the relative position of the source frequency band and the dissipation spectrum.

Shifting the source dominant frequency down to 10 kHz within the relaxation mechanism has also caused the slow *P* wave to be completely attenuated, even though porosity is the same (35 per cent) as in the previous example where the slow *P* wave was recorded.

The synthetic seismograms produced by exerting a fluid injection within the porous rock (Figs 11b and c) has wiped out the amplitudes of fast *P* and *S* waves for $\eta = 0.05$.

4.3 Fluid viscosity effects

The next case compares the effects of replacing water with gas, assuming $\eta = 25$ per cent and $f_0 = 100$ kHz (Fig. 12). The slow *P* wave has been completely attenuated regardless of the source type or the field variable, as expected. The presence of gas has caused a softening of the bulk of the rock, inducing an increase of amplitudes for the fast *P* wave when the source is applied either to the bulk of the material or only in the fluid. The opposite behaviour is observed when the measured internal field has been the result of fluid injection excitation. The amplitudes of the fast *S* wave are not affected by replacing water with gas, although it arrives slightly earlier. No trace of the slow *S* wave can be seen in these plots.

Replacing water with oil causes the fast *P* and *S* waves to have much larger amplitudes than with gas, but only when the source is applied to the bulk of the porous rock (Figs 13a–c) recorded as G_{11}^{mm} but much smaller when the source. Both waves have been delayed.

As discussed in Section 3.2, the kinematic properties of the slow *S* wave seem to indicate that when oil is fully saturating the porous medium, the wave could, in principle, propagate without dissipation within the low frequency band (Fig. 5d). This is because $Q^{\beta}_{\mathrm{slow}} > 100$ and $C^{\beta}_{\mathrm{slow}} \approx 400$ m s^{-1} for <100 kHz. This could represent an important tool for seismic exploration since the wave can be used for direct hydrocarbon detection. It should be noted that only those frequencies <10 kHz have the longest wavelengths (>10 cm), as depicted in Fig. 5(f).

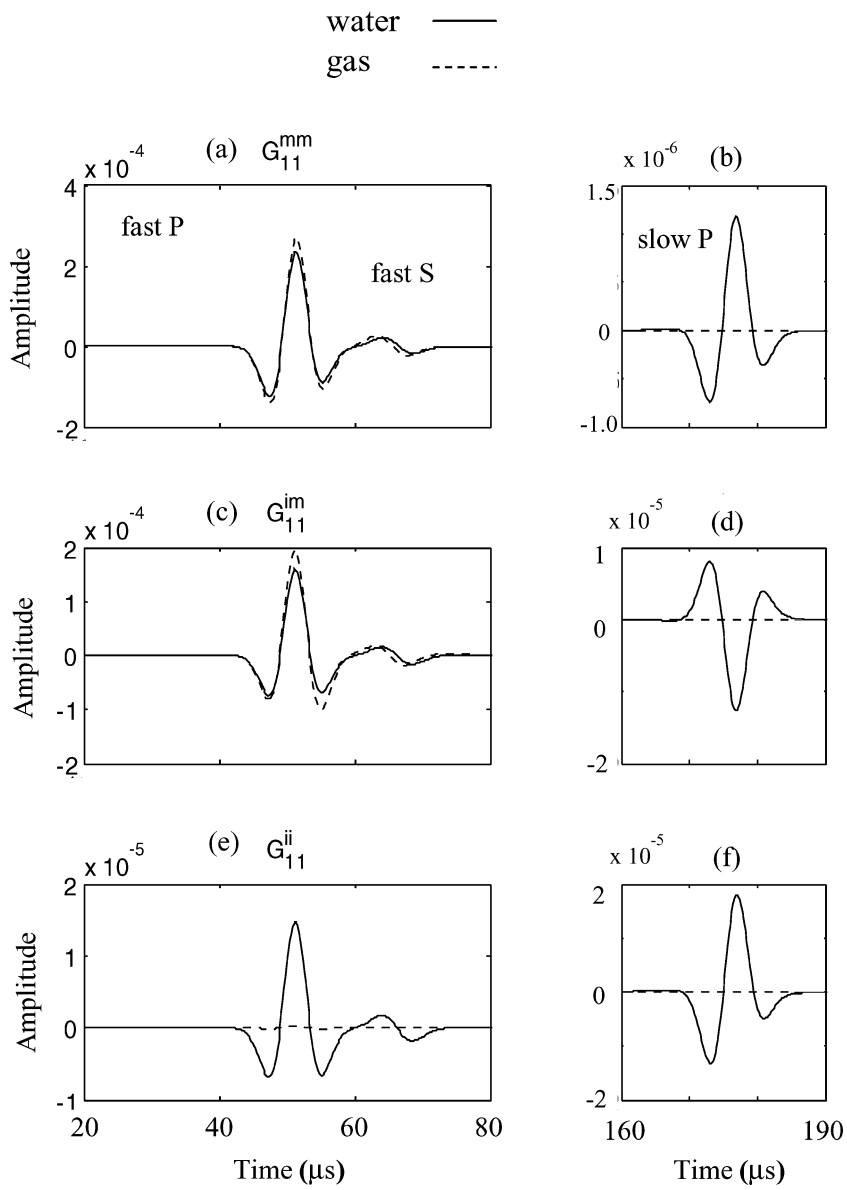


Figure 12. Synthetics computed for (a, b) G_{11}^{mm}, (c, d) G_{11}^{im} and (e, f) G_{11}^{ii} for a gas-saturated porous medium with $f_0 = 100$ kHz. They have been divided into two time-windows to enhance the amplitudes of the slow *P* wave. Source–receiver distance is 0.2 m. It compares the attenuation effects of decreasing fluid viscosity from water (solid line) to gas (dash).

However, even by focusing the source energy within the low frequency band, the slow *S* wave is not energetic enough to be recorded. This is shown in Fig. 14 where the slownesses of all four waves were calculated, assuming a spectrum bandwidth of $f_{max} = 3$ kHz ($f_0 = 1$ kHz). This frequency range spans wavelengths between 0.5 and 1 m (Fig. 4f). However, as can be observed in Fig. 14(d), the relative magnitude of the slow *S* wave slowness is nine orders of magnitude smaller than those of the fast *P* and *S* waves.

5 DISCUSSION AND CONCLUSIONS

It has been computed the dissipative characteristics of seismic waves in homogeneous isotropic fully saturated porous media within the general reformulated framework of Sahay theory. Quality factors and phase speeds were obtained, assuming homogeneous viscoelastic plane waves, in addition to the synthetic seismograms using the Green's function for a siliciclastic type of porous rock.

The results indicate that even though the amplitudes of the fast *P* and *S* waves in the theoretical seismograms of Sahay (2001) underwent attenuation, especially the slow *P* wave, it was not as strong as it could have been if the source and the dissipation spectra had overlapped fully, that is, the strongest frequency components of the source (10–316 kHz) were located beyond the peak of attenuation spectrum. As can be deduced from the phase speed and quality factors as a function of frequency (Fig. 3), it was only the lower frequency components the portion most affected by amplitude attenuation. This confirms that the longest offset waveforms in Sahay (2001) have retained the high-frequency phases. Minimal dispersion was experienced since the inflection point of the phase speed function was located far from the source spectrum. This hypothesis was confirmed by computing the Green's function for a source excitation whose peak frequency exactly overlapped the dissipation spectrum. Therefore, in this case the fast *P* and *S* waves experienced the strongest amplitude attenuation and

© 2007 The Authors, *GJI*, **170,** 1227–1242
Journal compilation © 2007 RAS

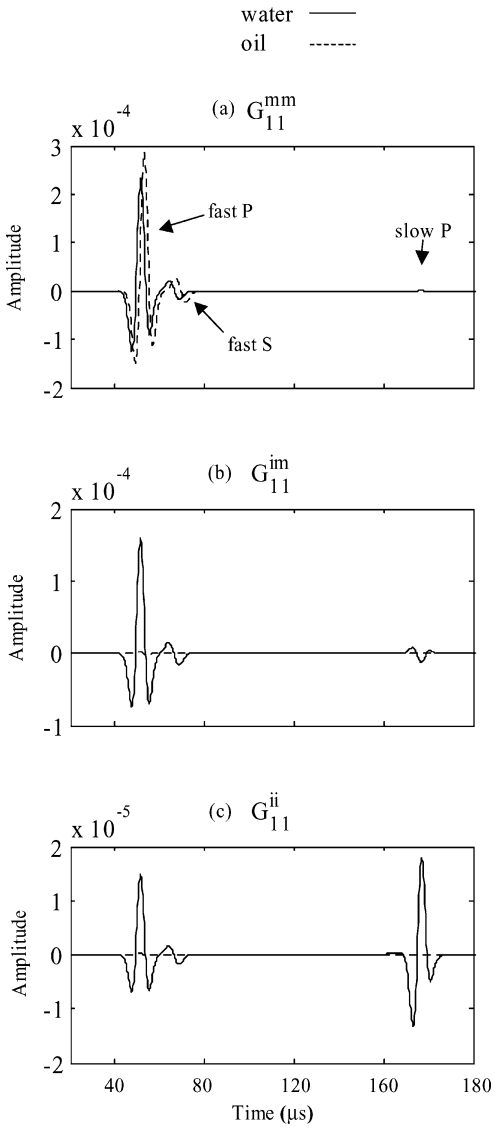


Figure 13. Synthetics computed for (a) G_{11}^{mm}, (b) G_{11}^{im} and (c) G_{11}^{ii} for an oil-saturated porous medium with $f_0 = 100$ kHz. Source–receiver distance is 0.2 m. It compares the attenuation effects of increasing fluid viscosity from water (solid) to oil (dash).

dispersion possible, given the specific physical parameters of the porous medium.

To calculate the amplitude attenuation and dispersion effects that seismic waves could experience with varying porosity and fluid viscosity, we aimed to compute the phase speeds and quality factors as a function of frequency for a sandstone type of porous rock. The results show, in general, that increasing porosity enhances dispersion and attenuation as expected, since viscous damping of seismic energy is associated to the presence of fluids through the two mechanisms modelled in de la Cruz and Spanos theory (Sahay 2001): Darcian attenuation and viscous dissipation of momentum within the fluid. However, since the seismic wavelength must be greater than the RVE so that a continuum description is firmly established, it is not clear whether it would be possible that the two mechanisms can be split into two distinct spectra, since a material point represents the coupling between the solid squeleton and the fluids.

When water saturates the porous medium, increasing pore space causes the relaxed phase speed of the fast *P* and fast *S* waves to slow down, especially that of slow *S* wave. The phase speed of the fast *S* wave at the high frequency limit (unrelaxed) increases with the amount of fluids. This result is, in principle, physically counterintuitive since it would be expected that the effective shear modulus of the porous rock be decreased as additional pore space is incorporated into the frame. However, increasing the amount of viscous fluids adds shear strength to the bulk of the porous rock, which might explain the increase in phase speed of the fast *P* wave at the unrelaxed limit.

As the amount of water was increased, so does the phase speed of the slow *P* wave and the window in which it becomes propagatory. Additionally, the dissipation spectrum of the slow *S* wave expands towards the low frequency band. This is in principle counterintuitive since it would be expected that by increasing the amounts of fluids, the slow shear wave, which exists due to the presence of viscous fluids, could propagate. However, as is discussed below, this may be the case for increasing fluid viscosity, rather than pore space.

Increasing fluid viscosity from gas to water to oil induces stronger attenuation as expected. It should be noted that as the amount of oil increases within the porous rock (porosity from 0.05 to 35 per cent), the wide relaxation spectrum observed when water fully saturates the porous medium, starts splitting into two distinct narrower spectra. They may be related to Darcian dissipation and viscous damping within the fluid, respectively. The Darcian relaxation peak is located at 10 MHz for both fast waves, whereas in the latter case, it is located at 50 MHz for the fast *P* wave and 3 GHz for the fast *S* wave. However, no physical significance may be attributed to the relaxation mechanism at higher frequencies since it is beyond the Poiseuille frequency limit regardless that the flow is compressible.

It was also observed that by replacing water for oil, the phase speed of the slow *S* wave increases and the relaxation spectrum shifts toward higher frequencies, leaving a window with $Q^{\beta}_{\text{slow}} \approx \infty$ in which it could propagate. This indicates, in principle, that the slow *S* wave could be used for direct hydrocarbon detection. However, the strength of the wave is orders of magnitude smaller to the other waves, as judged from the magnitude of its slowness. Therefore, from the theoretical point of view, is practically non-existent.

The results obtained in the present paper confirm that, within the frequency band modelled, it predicts sizeable levels of amplitude attenuation and velocity dispersion. However, it should be noted that being a dynamic problem, the solid δ_s and fluid δ_f compliances must be obtained through seismic dilatational motions, instead of using values calculated from static measurements, as was done in the present work. The main consequence is that dissipation may be slightly higher than obtained here.

It can be inferred from the numerical results that, within this band, the attenuation observed from the dynamic behaviour of seismic waves can be the result of the coupling between the flow of viscous fluids and the dynamic porosity. However, as attenuation studies of porosity relaxation are not well documented in the literature, nor the effects of bulk viscosity of fluids within the porous medium, it is not possible to draw quantitative conclusions.

Although the local changes of porosity (about its static value) are infinitesimally small (10^{-13}–10^{-14}), they are causing the flow of viscous fluids, that is, the relative fluid flow and the local fluid flows within the saturating fluids, to enhance attenuation. Therefore, it appears that there is no need to introduce physical heterogeneity or to include explicitly squirt-flow type of dissipation mechanisms to model realistic levels of attenuation within this frequency band.

An issue that remains unsolved is, nevertheless, to identify the dissipation mechanism(s) that cause(s) the attenuation and dispersion of seismic waves within the surface seismic frequency range, that is,

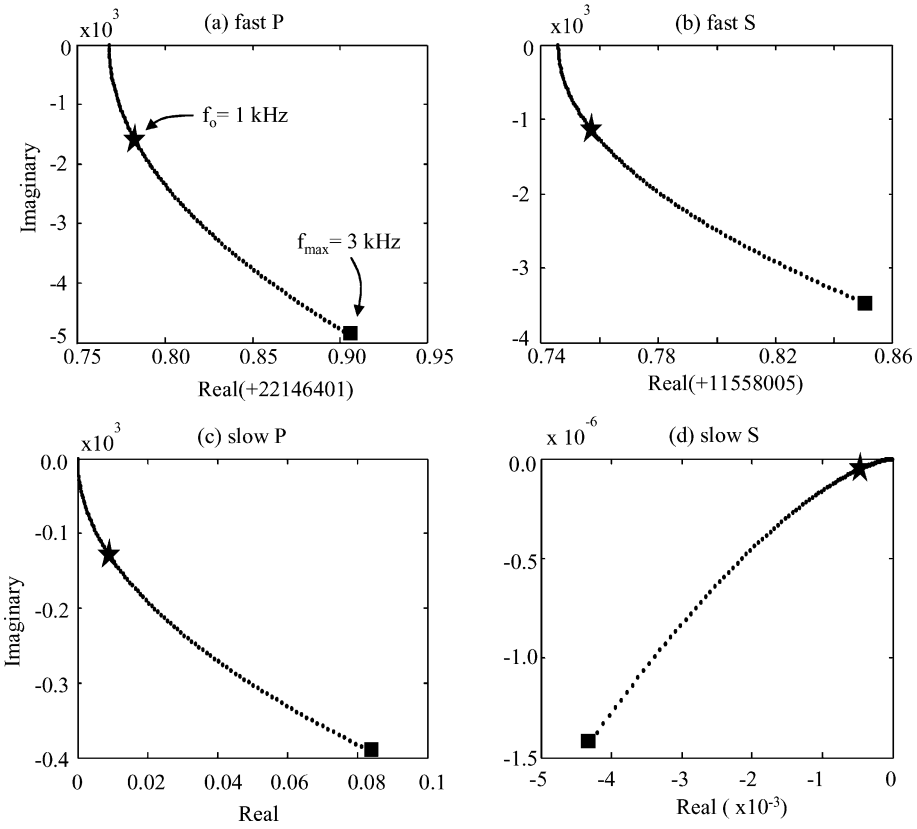


Figure 14. The real and imaginary parts of the complex slownesses of all four waves predicted in de la Cruz and Spanos theory (Sahay 2001). The bandwidth spans up to 3 kHz, which is the window where the slow *S* wave could become propagatory (Fig. 5).

$<$100 Hz. It is possible however, that physical inhomogeneities, that is, patchy or partial saturation, non-uniform porosity, etc. could shift or widen the dissipation enhanced by the local changes of porosity during wave propagation, towards lower frequencies.

ACKNOWLEDGMENTS

It is greatly appreciated the useful comments and suggestions made by the three reviewers and two editors to help improve the present work.

REFERENCES

Bhattacharyya, R.K., 1965. Rayleigh waves in granular medium, *Pure Appl. Geophys.,* **62,** 13–22.

Biot, M.A., 1956. Theory of propagation of elastic waves in a saturated porous solid, I, low-frequency range, *J. Acoust. Soc. Am.,* **29,** 168–178.

Biot, M.A., 1962. Mechanics of deformation and acoustic propagation in porous media, *J. Appl. Mech.,* **33,** 1482–1498.

Borcherdt, R.D. 1973. Energy and plane waves in linear viscoelastic media, *J. Geophys. Res.,* **78**(14), 2442–2453.

Bourbie, T., Coussy, O. & Zinszer, B., 1987. *Acoustics of Porous Media,* Gulf Publishing Co., Paris, France

Carcione, J.M. 2001. *Wave Fields in Real Media,* Pergamon, Amsterdam, the Netherlands.

Carcione, J.M., Helle, H.B. & Pham, N.H., 2003. White's model for wave propagation in partially saturated rocks: comparison with poroelastic numerical experiments, *Geophys.,* **68,** 1389–1398.

Carcione, J.M. & Quiroga-Goode, G., 1995. Some aspects of the physics and numerical modeling of Biot compressional waves, *J. Comp. Acoust.,* **3,** 261–280.

Carcione, J.M. & Quiroga-Goode, G., 1996. Full frequency-range transient solution for compressional waves in a fluid-saturated viscoelastic porous medium, *Geophys. Prosp.,* **44,** 99–129.

Corapcioglu M.Y. & Tuncay, K., 1996. *Propagation of Waves in Porous Media,* Chap. 5, Vol. 3, Advances in Porous Media, M.Y. Corapcioglu, Elsevier, Amsterdam.

de la Cruz, V. & Spanos, T.J.T., 1985. Seismic wave propagation in a porous medium, *Geophys.,* **50,** 1556–1565.

de la Cruz, V. & Spanos, T.J.T., 1989. Thermomechanical coupling during seismic wave propagation in a porous medium, *J. Geophys. Res.,* **94B,** 637–642.

de la Cruz, V., Sahay, P.N. & Spanos, T.J.T., 1993. Thermodynamics of porous media, *Proc. R. Soc. Lond. A,* **443,** 247–255.

Dvorkin, J. & Nur, A., 1993. Dynamic poroelasticity: a unified model with the squirt and the Biot mechanisms, *Geophys.,* **58,** 524–533.

Dvorkin, J., Nolen-Hoeksema, R. & Nur, A., 1994. The squirt-flow mechanism: macroscopic description, *Geophysics,* **59,** 428–438.

Gelinsky, S. & Shapiro, S.A., 1997. Dynamic equivalent medium approach for thinly layered saturated sediments, *Geophys. J. Int.,* **128,** F1–F4.

Godano, C. & Oliveri, F., 1999. Nonlinear seismic waves: a model for site effects, *Int. J. Non-Linear Mech.,* **34**(3), 457–468.

Gurevich, B., Zyrianov, V.B. & Lopatnikov, S.L., 1997. Seismic attenuation in finely layered porous rocks: effects of fluid flow and scattering, *Geophys.,* **62,** 319–324.

Helle, H.B., Pham, N.H. & Carcione, J.M., 2003. Velocity and attenuation in partially saturated rocks: poroelastic numerical experiments, *Geophys. Prosp.,* **51,** 551–566.

Hickey, C.J., 1994. Mechanics of porous media, *PhD thesis*, University of Alberta, Canada.

Hickey, C.J., Spanos, T.J.T. & de la Cruz, V., 1995. Deformation parameters of permeable media, *Geophys. J. Int.,* **121,** 359–370.

Mochizuki, S., 1982. Attenuation in partially saturated rocks, *J. Geophys. Res.,* **87,** 8598–8604.

Norris, A., 1993. Low-frequency dispersion and attenuation in partially saturated rocks, *J. Acoust. Soc. Am.,* **94,** 359–370.
Pride, S.R., Gangi, A.F. & Morgan, F.D., 1992. Deriving the equations of motion for porous isotropic media, *J. Acoust. Soc. Am.,* **92,** 3278–3290.
Pride, S.R., Berryman, J.G. & Harris, J.M., 2004. Seismic attenuation due to wave-induced flow, *J. Geophys. Res.,* **109,** B01201.
Rasolofosaon, P.N.J., 1991. Plane acoustic waves in linear viscoelastic porous media: energy, particle displacement, and physical interpretation, *J. Acoust. Soc. Am.,* **89,** 1532.
Quiroga-Goode, G., 2002a. Dynamics of Biot squirt-flow, 2002. *Acoust. Res. Lett. Online,* **3,** 12–17.
Quiroga-Goode, G., 2002b. Residual Strain in Biot Porous Media, *64th Conference of the Eur. Assoc. of Expl. Geophys. (EAGE) Florence,* Italy, P092.
Quiroga-Goode, G., Jiménez-Hernández, S., Flores-Pérez, M.A. & Padilla-Hernández, R., 2005. Computational studies of seismic waves in porous media with fluid and thermal relaxation: gauging Biot theory, *J. Geophys. Res.,* **110,** B07303.
Quiroga-Goode, G., Jiménez-Hernández, S. & Padilla-Hernández, R., 2006. Wave polarization in homogeneous composite media with pore relaxation, submitted to Geophys. *Res. Lett*.
Rasolofosaon, P., 1991. Plane acoustic waves in linear viscoelastic porous media: energy, particle displacement and physical interpretation, *J. Acoust. Soc. Am.,* **89,** 1532–1550.
Sahay, P.N., 1996. Elastodynamics of deformable porous media, *Proc. R. Soc. Lond. A,* **452,** 1517–1529.
Sahay, P.N., Spanos, T.J.T. & de la Cruz, V., 2001. Seismic wave propagation in inhomogeneous and isotropic porous media, *Geophys. J. Int.,* **145,** 209–222.
Sahay, P.N., 2001. Dynamic Green's function for homogeneous and isotropic porous media, *Geophys. J. Int.,* **147,** 622–629.
White, J.E., 1975. Computed seismic speeds and attenuation in rocks with partial gas saturation, *Geophys.,* **47,** 1–15.
Wilmanski, K., 2006. A few remarks on Biot's model and linear acoustics of poroelastic saturated materials, *Soil Dyn. Earthq. Eng.,* **26,** 509–536.
Zimmermann, R.W., 1991. *Compressibility of Sandstones,* Elsevier Science, Amsterdam, the Netherlands.

APPENDIX A: POROELASTIC CONSTANTS

The poroelastic constants are rearranged here (from Sahay 1996),

$$K_{\rm mm}^{\rm Re} = (\phi - \delta_{\rm s} + \delta_{\rm f})K_{\rm s} + (\eta - \delta_{\rm s} - \delta_{\rm f})K_{\rm f}$$

$$K_{\rm mm}^{\rm Im} = (\eta - \delta_{\rm s} - \delta_{\rm f})\xi_{\rm f}$$

$$K_{\rm mi}^{\rm Re} = \left[\frac{\rho_{\rm f}^{\rm m}}{\rho}(\phi - \delta_{\rm s}) - \frac{\rho_{\rm s}^{\rm m}}{\rho}\delta_{\rm f}\right]K_{\rm s} + \left[\frac{\rho_{\rm f}^{\rm m}}{\rho}\delta_{\rm s} - \frac{\rho_{\rm s}^{\rm m}}{\rho}(\eta - \delta_{\rm f})\right]K_{\rm f}$$

$$K_{\rm mi}^{\rm Im} = \left[\frac{\rho_{\rm f}^{\rm m}}{\rho}\delta_{\rm s} - \frac{\rho_{\rm s}^{\rm m}}{\rho}(\eta - \delta_{\rm f})\right]\xi_{\rm f}$$

$$K_{\rm im}^{\rm Re} = \left[\frac{\rho_{\rm f}^{\rm m}}{\rho}(\phi - \delta_{\rm s} + \delta_{\rm f})K_{\rm s} - \frac{\rho_{\rm s}^{\rm m}}{\rho}(\eta + \delta_{\rm s} - \delta_{\rm f})\right]K_{\rm f}$$

$$K_{\rm im}^{\rm Im} = -\left[\frac{\rho_{\rm s}^{\rm m}}{\rho}(\eta + \delta_{\rm s} - \delta_{\rm f})\right]\xi_{\rm f}$$

$$K_{\rm ii}^{\rm Re} = \frac{\rho_{\rm f}^{\rm m}}{\rho^2}\left[\rho_{\rm f}^{\rm m}(\phi - \delta_{\rm s}) - \rho_{\rm s}^{\rm m}\delta_{\rm f}\right]K_{\rm s} - \frac{\rho_{\rm s}^{\rm m}}{\rho^2}\left[\rho_{\rm f}^{\rm m}\delta_{\rm s} - \rho_{\rm s}^{\rm m}(\eta - \delta_{\rm f})\right]K_{\rm f}$$

$$K_{\rm ii}^{\rm Im} = -\frac{\rho_{\rm s}^{\rm m}}{\rho^2}\left[\rho_{\rm f}^{\rm m}\delta_{\rm s} - \rho_{\rm s}^{\rm m}(\eta - \delta_{\rm f})\right]\xi_{\rm f}$$

$$\mu_{\rm mm}^{\rm Re} = (\phi + \delta_{\rm m})\mu_{\rm s}$$

$$\mu_{\rm mm}^{\rm Im} = (\eta - \delta_{\rm m})\mu_{\rm f}$$

$$\mu_{\rm mi}^{\rm Re} = \frac{\rho_{\rm f}^{\rm m}}{\rho}(\phi - \delta_{\rm m})\mu_{\rm s}$$

$$\mu_{\rm mi}^{\rm Im} = \frac{\eta}{\rho}\left[\rho_{\rm f}\delta_{\mu} + \rho_{\rm s}^{\rm m}\right]\mu_{\rm f}$$

$$\mu_{\rm im}^{\rm Re} = \mu_{\rm mi}^{\rm Re}$$

$$\mu_{\rm im}^{\rm Im} = -\frac{\rho_{\rm s}^{\rm m}}{\rho}(\eta - \delta_{\mu})\mu_{\rm f}$$

$$\mu_{\rm ii}^{\rm Re} = \frac{\rho_{\rm f}^{\rm m}}{\rho}\frac{\rho_{\rm f}^{\rm m}}{\rho}(\phi + \delta_{\mu})\mu_{\rm s}$$

$$\mu_{\rm ii}^{\rm Im} = \frac{\rho_{\rm r}}{\rho_{\rm f}\rho}\left[\rho_{\rm f}\delta_{\mu} + \rho_{\rm s}^{\rm m}\right]\mu_{\rm f}$$

with $\phi = 1 - \eta$. The superscripts Re and Im stand for the real and the imaginary parts of the corresponding material property. The parameter $\xi_{\rm f}$ corresponds to the bulk fluid viscosity, which is related to the fluid shear viscosity $\mu_{\rm f}$ by $\xi_{\rm f} = \lambda_{\rm f} + \frac{2}{3}\mu_f$ where $\lambda_{\rm f}$ is analogous to the first Lamé constant.

The dimensionless parameters $\delta_{\rm s}$ and $\delta_{\rm s}$ correspond to the solid and fluid compliances, respectively. They are empirical constants whose values depend on the process under consideration. For low frequency seismic propagation, they can be defined as (Hickey 1994):

$$\delta_{\rm s} = \eta[K_{\rm f}(K_{bc} - \eta K_{bp})]\zeta^{-1},$$

and

$$\delta_{\rm f} = \eta[K_{bp}(\phi K_{\rm s} - K_{bc})]\zeta^{-1},$$

where $\zeta = \eta K_{bp}(K_{\rm f} - K_{\rm s}) + K_{\rm f}K_{bc}$. The constants K_{bp} and K_{bc} correspond to the drained compressibility (bulk modulus) and pseudo-bulk compressibility, respectively. And finally, the macroscopic and the solid shear moduli are related by $\mu_{\rm M} = (1 - \eta)(1 - \delta_{\mu})\,\mu_{\rm s}$.

APPENDIX B: MATERIAL PROPERTIES OF THE POROUS MEDIUM

The material properties of a porous material similar to Berea sandstone saturated with water and oil (Hickey 1994).

Solid								Units
η	0.05	0.10	0.15	0.20	0.25	0.30	0.35	
K	0.002	0.160	0.700	1.7	3	5	7	Darcy
$\mu_{\rm M}$	11e9	7e9	4e9	3e9	2e9	1.5e9	1.e9	Pa
$K_{\rm b}$	50e9	36e9	25e9	20e9	14e9	10e9	10e9	Pa
$K_{\rm bc}$	7.1e9							Pa
$K_{\rm s}$	3.3e10							Pa
$\mu_{\rm s}$	2.3e10							Pa
ρ_{12}	-83							kg m^{-3}
$\rho_{\rm s}$	2650							kg m^{-3}
Fluid	Water	Oil	Gas					Units
$\rho_{\rm f}{}^{\circ}$	1000	1100	10					kg m^{-3}
$K_{\rm f}$	2.2e9	2.0e9	1.44e6					Pa
$\mu_{\rm f}$	1e–3	1.e0	2.20e–5					Pa s
$\xi_{\rm f}$	2.8e–3	10e0	6e–5					Pa s

© 2007 The Authors, *GJI*, **170,** 1227–1242
Journal compilation © 2007 RAS